ACS APPLIED MATERIALS & INTERFACES

Letter

www.acsami.org

Novel Approach to the Preparation of Organic Energetic Film for Microelectromechanical Systems and Microactuator Applications

Jun Wang,[†] Wenchao Zhang,*[,†] Lianwei Wang,[‡] Ruiqi Shen,[†] Xing Xu,[†,§] Jiahai Ye,[†] and Yimin Chao*[,∥]

[†]School of Chemical Engineering, Nanjing University of Science and Technology, Nanjing 210094, China

[‡]Key Laboratory of Polar Material and Device and Department of Electronic Engineering, East China Normal University, Shanghai 200241, China

[§]Aerospace Haiying (Zhenjiang) Special Materials Co. Ltd., Zhenjiang 212132, China

[∥]School of Chemistry, University of East Anglia, Norwich NR4 7TJ, United Kingdom

Supporting Information

ABSTRACT: An activated RDX−Fe_2O_3 xerogel in a Si-microchannel plate (MCP) has been successfully prepared by a novel propylene epoxide-mediated sol−gel method. A decrease of nearly 40 °C in decomposition temperature has been observed compared with the original cyclotrimethylene trinitramine (RDX). The RDX−Fe_2O_3 xerogel can release gas and solid matter simultaneously, and the ratio of gas to solid can be tailored easily by changing the initial proportions of RDX and $FeCl_3{\cdot}6H_2O$, which significantly enhances the explosive and propulsion effects and is of great benefit to the applications. The approach, which is simple, safe, and fully compatible with MEMS technology, opens a new route to the introduction of organic energetic materials to a silicon substrate.

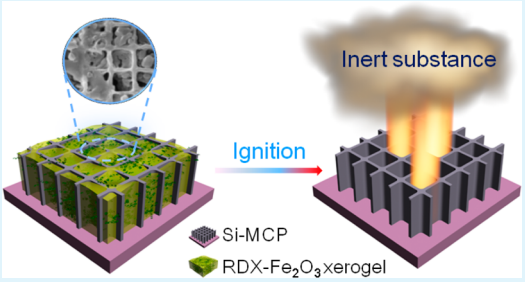

KEYWORDS: *nanoscale RDX, silicon microchannel plate, microactuator, MEMS, energetic materials*

With the diversity in function in microelectromechanical system (MEMS) devices, it is more and more difficult to meet the growing need of power with batteries. Their limited energy density is driving the emergence of a new class of power MEMS.[1,2] Energetic materials are defined as a class of substances that store chemical energy and generate gas, heat, and power rapidly when they are fired.[3−5] Their performances can be tailored by changing the stoichiometry and sizes of the chemical reactants, which is a key to great advances in power MEMS, such as micropropeller, microactuator, microinitiation, and other microsystems.[6] Considering the compatibility of the energetic materials with MEMS technologies, nanothermite and energetic nanoporous silicon are usually used as energy for power MEMS. Many efforts have focused on MEMS devices that have been integrated with nanothermite by deposition onto silicon substrates, which is a widely used technique in MEMS research. In these processes, the oxidizer (e.g., NiO,[7] CuO,[8] and Ni[9]) is first integrated onto the silicon substrate, and subsequently the fuel (e.g., Al) is introduced to the oxidizer by thermal evaporation or sputter deposition. The energetic materials fabricated using these approaches have numerous advantages such as higher combustion velocity, lower ignition temperature, shorter ignition delay, and tailored dimensions when compared with conventional approaches.[10] However, a small amount of gas products of thermites reduce the potential diversity of functionality in resultant MEMS devices. Several previous papers have reported that nanoscale silicon can serve as a fuel when combined with a source of oxygen.[11−14] The reactions of sponge-like nanoporous silicon with liquid oxygen or oxygen-containing salts (e.g., metal nitrates and metal perchlorate) are strongly exothermic, but the long-term storage stability of energetic nanoporous silicon must be addressed.

Extensive amounts of research have been reported regarding nanothermite and energetic nanoporous silicon in terms of integration onto silicon substrates.[15] However, limited research has been undertaken into gas-generating materials, especially organic energetic materials that have been added to silicon substrates. Nevertheless, several recent papers addressing this issue indicate that gas generation plays an important role in the altitude control of orbiting microspacecraft and in microscale devices capable of producing tens of milliNewtons (mN) of thrust.[16,17] In our work, a silicon microchannel plate (Si-MCP) was prepared by photoelectrochemical etching. A gas-generating explosive, cyclotrimethylene trinitramine (RDX), was then loaded into the pores of the Si-MCP matrix using a sol−gel method. The sol−gel method involves reactions in solution to produce dispersion of nanoparticles in a liquid phase, called "sol". Through condensation, the sol gives a 3-D solid network, called a "gel", with the open pores being occupied by the solvent.[6] Finally, a RDX−Fe_2O_3 xerogel/Si-MCP composite was obtained after placing the Si-MCP loaded with the RDX−Fe_2O_3 xerogel composite in an oven for 72 h at

Received: May 9, 2014
Accepted: July 5, 2014
Published: July 6, 2014

   dx.doi.org/10.1021/am5028617 | *ACS Appl. Mater. Interfaces* 2014, 6, 10992−10996

60 °C. Compared with all the technologies discussed above this method is simpler, safer, applicable to other organic energetic materials, and of lower cost.

The source silicon wafer was P-type (100) oriented with a resistivity of 2−8 Ω·cm and a thickness of 525 μm. RDX was supplied by the Institute of Chemical Materials, CAEP. Ferric chloride hexahydrate ($FeCl_3·6H_2O$), *N*,*N*-dimethylformamide (DMF), and propylene oxide were obtained from Aladdin-Reagent Inc. and used as received.

Si-MCP, with one end open, was produced by photoelectrochemical etching as in our previous work.[18−20] The backside of the silicon wafer, which served as a substrate in our research, was not removed after anodization. The Si-MCP sample was cut into squares with dimensions of approximately 5 × 5 mm using a 200 W CO_2 laser. The synthesis of nanoscale RDX is possible with sol−gel processing.

Fabrication of the activated RDX−Fe_2O_3 xerogel/Si-MCP composite is illustrated in Scheme 1. Amounts of 1.57 mmol of

Scheme 1. Fabrication of the Activated RDX−Fe_2O_3 Xerogel/Si-MCP Composite

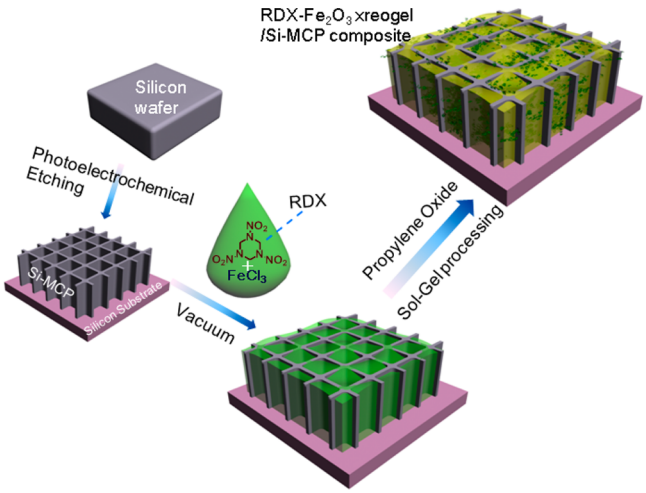

$FeCl_3·6H_2O$ and 1.13 mmol of RDX were sequentially added to 2.0 mL of DMF until they were completely dissolved to form a clear red-orange solution, which remained unchanged upon storage. Si-MCP was then immersed in this solution for 5 min under vacuum. Finally, 1.3 mL of propylene oxide was dropped into the solution leading to the hydrolysis of $FeCl_3·6H_2O$ around RDX; the solution transformed into a rigid red-brown gel after 1.5 h. The impregnated Si-MCP was then separated and placed in the oven at 60 °C for 72 h to produce the RDX−Fe_2O_3 xerogel/Si-MCP composite.

During sol−gel processing RDX was entrapped within the pores of the wet monolithic gel, which restrained the crystallization growth of RDX particles beyond the nanometer or submicron scales.[21−23]

The surface and cross-section morphologies of Si-MCP without and with the activated RDX−Fe_2O_3 xerogel composite were examined by scanning electron microscopy (SEM, Hitachi, S4800). A piece of RDX−Fe_2O_3 xerogel/Si-MCP composite was peeled from the silicon substrate for thermogravimetric analysis and differential scanning calorimetry (TGA-DSC, Mettler Toledo). The TGA-DSC experiment was carried out between the range of 100 and 350 °C at a heating rate of 15 °C·min^{-1} under a N_2 flow of 20 mL·min^{-1}. X-ray diffraction (XRD, Bruker D8 Advance) was carried out to determine the crystalline nature of the RDX−Fe_2O_3 xerogel/Si-MCP composite before and after TGA-DSC testing. The ignition property of this composite was monitored and recorded using a high-speed camera running at 2500 fps.

In Figure 1, SEM images show the top view and the cross-section of Si-MCP before and after filling with the activated

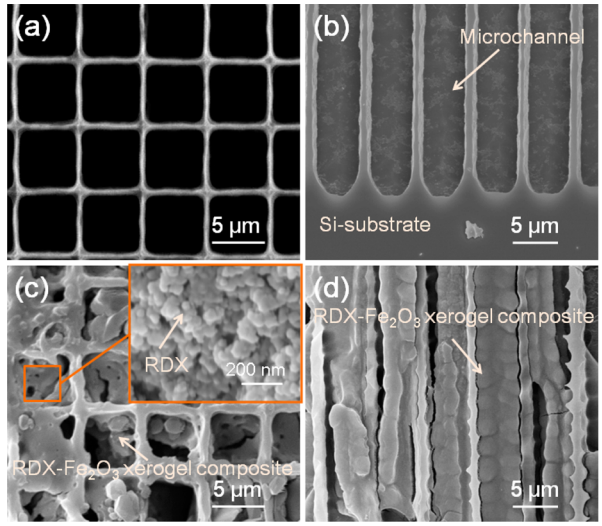

Figure 1. SEM images of the Si-MCP before filling with RDX−Fe_2O_3 xerogel composite: (a) top view; (b) cross-section view. SEM images of the Si-MCP after filling with the RDX−Fe_2O_3 xerogel composite: (c) top view; and (d) cross-section view. Inset in (c) shows the detailed morphology of the RDX−Fe_2O_3 xerogel composite.

RDX−Fe_2O_3 xerogel composite. From these images in Figure 1a and b, one can see that the silicon microchannels were highly ordered and had square pores of 5 μm in size. The walls of the pores were smooth and straight before being filled with the RDX−Fe_2O_3 xerogel composite. The morphologies of the surface and the channels changed considerably after filling with the RDX−Fe_2O_3 xerogel composite. Figure 1c and d show that the composite was intimately combined with the silicon microchannel, and thus the composite was loaded successfully within the Si-MCP. This special microchannel structure effectively prevented the composite from breaking off. The detailed morphology of the RDX−Fe_2O_3 xerogel composite is shown in the inset of Figure 1c. The average particle size of RDX, which was restricted by the size of the microchannels of the Fe_2O_3 gel network skeleton, was approximately 50 nm. (More information about RDX−Fe_2O_3 xerogel composite can be found in the Supporting Information.) Combining SEM images with FTIR spectra in Figure S3 (Supporting Information), we can summarize that Fe_2O_3 xerogel mixed with nanoscale RDX had been synthesized successfully.

Figure 2a shows the TGA curve of the RDX−Fe_2O_3 xerogel/Si-MCP. Up to 189 °C, the weight loss of approximately 14.5% is due to the evaporation of bonded water and DMF residue in the sample. A sudden weight loss of more than 53.6% was observed between 189 and 210 °C. This percentage is significantly larger than the theoretical weight percentage (<37%) of RDX in the RDX−Fe_2O_3 xerogel/Si-MCP. This weight loss was attributed to the rapid decomposition of RDX resulting in N_2, water vapor, and oxocarbon and the Fe_2O_3 xerogel being removed from the silicon microchannel upon gas generation. A meticulous XRD (Figure 2c) did not reveal any

dx.doi.org/10.1021/am5028617 | ACS Appl. Mater. Interfaces 2014, 6, 10992−10996

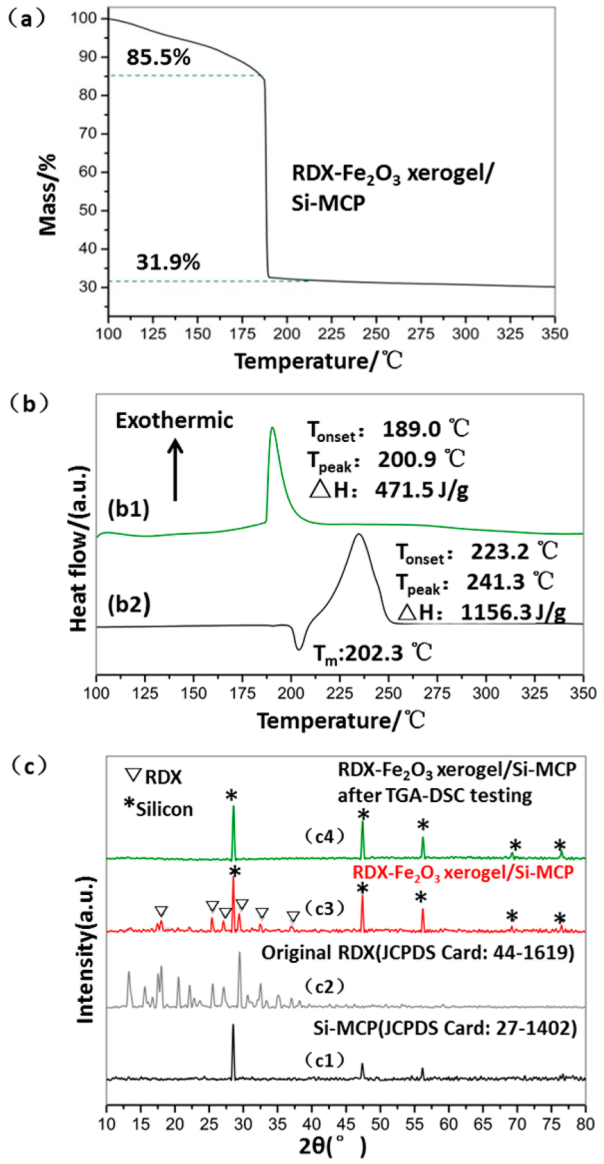

Figure 2. (a) TGA curves of the RDX−Fe_2O_3 xerogel/Si-MCP; (b) DSC curves for (b1) the original RDX and (b2) the RDX−Fe_2O_3 xerogel/Si-MCP; (c) XRD patterns of (c1) Si-MCP, (c2) original RDX, (c3) RDX−Fe_2O_3 xerogel/Si-MCP, and (c4) RDX−Fe_2O_3 xerogel/Si-MCP after DSC testing.

presence of Fe_2O_3, thus it was concluded that the Si-MCP skeleton did not have residual Fe_2O_3 after TGA-DSC testing.

Figure 2b shows a comparison between the DSC curves of the original RDX and the RDX−Fe_2O_3 xerogel/Si-MCP. The original RDX exhibited a strong exothermic peak (T_{peak}) at 241.3 °C and a relatively lower endothermic peak (T_m) at 202.3 °C. This proved that the decomposition of RDX occurred after it melted. However, no endothermic peak was observed for RDX melting on the DSC curve of the RDX−Fe_2O_3 xerogel/Si-MCP. Interestingly, it was noticed that a dramatic shift in the decomposition temperature of the RDX prepared using this sol−gel method occurred, which is nearly 40 °C less than that of the original RDX. This means that the RDX decomposed before it melted. The large decrease of decomposition temperature of the RDX is shown to be caused by two factors: the presence of Fe^{3+} ions in the Fe_2O_3 xerogel and the size of the RDX particles. First, the presence of Fe^{3+} ions in the Fe_2O_3 xerogel can generate a coordination bond with the $-NO_2$ in the RDX, which accelerates the break of the N−NO_2 bond and promotes the decomposition reaction,[24,25] and second, the size of RDX particles in the RDX−Fe_2O_3 xerogel/Si-MCP, shown in Figure 1c, was restricted to the nanoscale due to the size of the microchannels of the Fe_2O_3 gel network skeleton. Compared with the original RDX, nano RDX particles have a larger part of atoms distributing on the surface of the crystals, which has a greater influence on the properties of nano-energetic material, such as the decomposition temperature.[26]

The Fe_2O_3 xerogel has not previously been known to catalyze the thermal decomposition of RDX to such a great extent, and the results achieved occurred only when specific material properties were met. Although our methodological study has not yet provided a complete characterization to fully document the potential of the Fe_2O_3 xerogel-based RDX for optimal performance, it paves the way to a new route for the fabrication of activated nanosized RDX with precise control through sol−gel processing.

A further comparison between these two DSC curves indicated that the exothermic heat (ΔH: 471.5 $J \cdot g^{-1}$) of the RDX−Fe_2O_3 xerogel/Si-MCP was much lower than that of the original RDX (ΔH: 1156.3 $J \cdot g^{-1}$). The large difference in energy output may be related to the coexistence of the inert materials: silicon and Fe_2O_3 xerogel.

All the samples were finely ground using an agate mortar for XRD characterization. XRD patterns of the RDX−Fe_2O_3 xerogel/Si-MCP before and after DSC testing are shown in Figure 2c. For reference, the XRD patterns of Si-MCP and RDX are also shown in Figure 2c1 and c2. The crystal phases of both compounds were consistent with the standard XRD data for Si-MCP (JCPDS card 27-1402) and RDX (JCPDS card 44-1619). However, the relative peak height of the RDX in the composite was much lower than that of the original RDX. The decrease in intensities can be attributed to the dominance of silicon diffraction, the lower concentration of RDX, as well as the decrease in RDX crystallinity and particle size. The XRD patterns and SEM images of Si-MCP with and without RDX−Fe_2O_3 xerogel gave clear evidence of substantial filling of silicon microchannels with the RDX−Fe_2O_3 xerogel composite. Furthermore, it was difficult to detect the XRD peaks of Fe_2O_3 in the composite because the product of the propylene

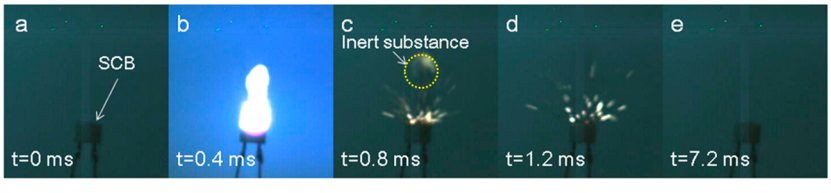

Figure 3. Sequence of images that shows gas generation as well as an inert substance. (a) SCB equipment, (b) triggering of the RDX−Fe_2O_3 xerogel/Si-MCP, (c) inert smoke generated, (d) inert smoke dissipates, (e) after ignition.

oxide catalyzed gelation of $Fe(H_2O)_6^{3+}$ was mainly an amorphous iron oxide/hydroxide phase known as ferrihydrite.[27] Heat treatment of the amorphous xerogel at 300 °C under an inert gas flow leads to the formation of hematite (α-Fe_2O_3).[23] However, there was no XRD pattern indicating the presence of hematite in the Si-MCP of RDX−Fe_2O_3 xerogel/Si-MCP after the DSC analysis. This was due to monoliths fragmenting into powder upon the decomposition of RDX and the gaseous species rushing out of the microchannels together with these fragments. An integrated analysis of the TGA and XRD characteristics further showed that the xerogel was removed from the silicon microchannel as the gas was generated.

A semiconductor bridge (SCB) was used to ignite the fabricated sample. The gas generation procedure was monitored and recorded with a high speed camera at a rate of 2500 fps. A very bright flash is clearly visible in Figure 3b, and this confirmed that the sample was successfully triggered. The ball of smoke in Figure 3c is likely from an inert substance.

The nature of the RDX−Fe_2O_3 xerogel/Si-MCP structure was an assembly of many microartillery units arranged in an ordered manner on a substrate, and the Fe_2O_3 xerogel splinters acted as bullets. The specially designed silicon walls separated the RDX−Fe_2O_3 xerogel, and the substrate was closed on one side of the microchannel, which can help the gaseous species rush out from the open window side. Directional flying splinters from the Fe_2O_3 xerogel, which are capable of producing tens of millinewtons of thrust, can greatly improve the explosive and propulsion effects (see Graphic Table of Content). This function is widely used in the altitude control of orbiting microspacecraft and the ignition of microscale devices. Furthermore, the ratio of gas to "bullets" production can also be tailored by changing the initial proportions of RDX and $FeCl_3{\cdot}6H_2O$. The presence of more RDX in the composite leads to the release of a larger amount of gas, facilitating a propellant application. Conversely, by increasing the Fe_2O_3 xerogel in the matrix pores to an optimal proportion, a composite that is more suitable for ignition reliability of microscale devices, microexplosive cutting, and separation and other applications can be produced.

In summary, activated RDX−Fe_2O_3 xerogel in the Si-MCP has been successfully synthesized by the epoxide-mediated sol−gel approach, which opens a new route to the introduction of organic energetic materials to a silicon substrate. From a synthetic point of view, the ability to form nanoscale organic energetic film from a simple sol in a controllable fashion results in both simpler synthesis due to less required instrumentation and greater safety, as the process does not rely on high temperature, pressure, or mechanical force. Since the microchannel structure of Si-MCP is open at one end and RDX−Fe_2O_3 xerogel can release gaseous fluid and inert substances simultaneously, the activated RDX−Fe_2O_3 xerogel in the Si-MCP can greatly enhance the explosive and propulsion effects. It is advantageous to the altitude control of orbiting microspacecraft and the ignition reliability of microscale devices. This method, fully compatible with MEMS technology, will significantly facilitate more research into gas-producing MEMS devices for microactuators and for other applications.

In addition, the synergy gained from network skeleton xerogel and Fe^{3+} ions has dramatically accelerated the thermal decomposition of RDX, which has caused the endothermic peak for RDX melting to disappear, and the decomposition temperature shifted from 241.3 to 200.9 °C. Due to the reduction of ignition energy required, the ignition reliability of microscale devices can be improved significantly.

■ ASSOCIATED CONTENT

Supporting Information

Photographs of RDX−Fe_2O_3 xerogel/Si-MCP composite and RDX−Fe_2O_3 xerogel composite, EDX analysis of RDX−Fe_2O_3 xerogel composite, and FTIR spectra analysis. This material is available free of charge via the Internet at http://pubs.acs.org.

■ AUTHOR INFORMATION

Corresponding Authors

*E-mail: zhangwenchao303@aliyun.com (W.Z.)
*E-mail: y.chao@uea.ac.uk (Y.C.).

Notes

The authors declare no competing financial interest.

■ ACKNOWLEDGMENTS

This work is supported by the National Science Foundation of China (NSFC) under grant numbers 50806033 and 61176108 and Chinese Postdoctoral Science Foundation under grant number 2012M511285. Mr Fred Huld is thanked for critical proof reading and discussions.

■ REFERENCES

(1) Chou, S.; Yang, W.; Chua, K.; Li, J.; Zhang, K. Development of Micro Power Generators−a Review. *Appl. Energy* **2011**, *88* (1), 1−16.
(2) Zhang, W.; Xu, B.; Wang, L.; Wang, X.; Thomas, J.; Chao, Y. Synthesis of Nickel Picrate Energetic Film in a 3d Ordered Silicon Microchannel Plate through an in Situ Chemical Reaction. *J. Mater. Sci.* **2013**, *48* (23), 8302−8307.
(3) Kim, S. H.; Zachariah, M. R. Enhancing the Rate of Energy Release from Nanoenergetic Materials by Electrostatically Enhanced Assembly. *Adv. Mater.* **2004**, *16* (20), 1821−1825.
(4) Reddy, B.; Das, K.; Das, S. A Review on the Synthesis of in Situ Aluminum Based Composites by Thermal, Mechanical and Mechanical−Thermal Activation of Chemical Reactions. *J. Mater. Sci.* **2007**, *42* (22), 9366−9378.
(5) Yang, Y.; Xu, D.; Zhang, K. Effect of Nanostructures on the Exothermic Reaction and Ignition of Al/Cuox Based Energetic Materials. *J. Mater. Sci.* **2012**, *47* (3), 1296−1305.
(6) Rossi, C.; Zhang, K.; Esteve, D.; Alphonse, P.; Tailhades, P.; Vahlas, C. Nanoenergetic Materials for Mems: A Review. *J. Microelectromech. Syst.* **2007**, *16* (4), 919−931.
(7) Wen, J. Z.; Ringuette, S.; Bohlouli-Zanjani, G.; Hu, A.; Nguyen, N. H.; Persic, J.; Petre, C. F.; Zhou, Y. N. Characterization of Thermochemical Properties of Al Nanoparticle and Nio Nanowire Composites. *Nanoscale Res. Lett.* **2013**, *8* (1), 1−9.
(8) Zhang, K.; Rossi, C.; Ardila Rodriguez, G. A.; Tenailleau, C.; Alphonse, P. Development of a Nano-Al/Cuo Based Energetic Material on Silicon Substrate. *Appl. Phys. Lett.* **2007**, *91* (11), 113−117.
(9) Jin, X.; Hu, Y.; Wang, Y.; Shen, R.; Ye, Y.; Wu, L.; Wang, S. Template-Based Synthesis of Ni Nanorods on Silicon Substrate. *Appl. Surf. Sci.* **2012**, *258* (7), 2977−2981.
(10) Zhang, W.; Yin, B.; Shen, R.; Ye, J.; Thomas, J. A.; Chao, Y. Significantly Enhanced Energy Output from 3d Ordered Macroporous Structured Fe_2o_3/Al Nanothermite Film. *ACS Appl. Mater. Interfaces* **2013**, *5* (2), 239−242.
(11) Kovalev, D.; Timoshenko, V. Y.; Künzner, N.; Gross, E.; Koch, F. Strong Explosive Interaction of Hydrogenated Porous Silicon with Oxygen at Cryogenic Temperatures. *Phys. Rev. Lett.* **2001**, *87* (6), 683011−683014.
(12) Mikulec, F. V.; Kirtland, J. D.; Sailor, M. J. Explosive Nanocrystalline Porous Silicon and Its Use in Atomic Emission Spectroscopy. *Adv. Mater.* **2002**, *14* (1), 38−41.

(13) Becker, C. R.; Apperson, S.; Morris, C. J.; Gangopadhyay, S.; Currano, L. J.; Churaman, W. A.; Stoldt, C. R. Galvanic Porous Silicon Composites for High-Velocity Nanoenergetics. *Nano Lett.* **2010**, *11* (2), 803−807.
(14) Malec, C. D.; Voelcker, N. H.; Shapter, J. G.; Ellis, A. V. Carbon Nanotubes Initiate the Explosion of Porous Silicon. *Mater. Lett.* **2010**, *64* (22), 2517−2519.
(15) Zhou, X.; Torabi, M.; Lu, J.; Shen, R.; Zhang, K. Nanostructured Energetic Composites: Synthesis, Ignition/Combustion Modeling, and Applications. *ACS Appl. Mater. Interfaces* **2014**, *6* (5), 3058−3074.
(16) Zhang, W.; Peng, H.; Gao, X.; Ye, J.; Zhang, Z.; Chao, Y. An in Situ Chemical Reaction Approach to Synthesize Zinc Picrate Energetic Thin Film Upon Zinc Oxide Nanowires Array. *Surf. Interface Anal.* **2012**, *44* (8), 1203−1208.
(17) DiBiaso, H. H.; English, B. A.; Allen, M. G. Solid-Phase Conductive Fuels for Chemical Microactuators. *Sens. Actuators, A* **2004**, *111* (2−3), 260−266.
(18) Carlson, T. R.; Vispute, T. R.; Huber, G. W. Green Gasoline by Catalytic Fast Pyrolysis of Solid Biomass Derived Compounds. *ChemSusChem* **2008**, *1* (5), 397−400.
(19) Chen, X. M.; Lin, J. L.; Yuan, D.; Ci, P. L.; Xin, P. S.; Xu, S. H.; Wang, L. W. Obtaining a High Area Ratio Free-Standing Silicon Microchannel Plate Via a Modified Electrochemical Procedure. *J. Micromech. Microeng.* **2008**, *18* (3), 1−4.
(20) Yuan, D.; Ci, P. L.; Tian, F.; Shi, J.; Xu, S. H.; Xin, P. S.; Wang, L. W.; Chu, P. K. Large-Size P-Type Silicon Microchannel Plates Prepared by Photoelectrochemical Etching. *J. Micro/Nanolithogr., MEMS, MOEMS* **2009**, *8* (3), 033012.
(21) Tillotson, T. M.; Hrubesh, L. W.; Simpson, R. L.; Lee, R. S.; Swansiger, R. W.; Simpson, L. R. Sol-Gel Processing of Energetic Materials. *J. Non-Cryst. Solids* **1998**, *225* (1), 358−363.
(22) Chen, R. J.; Luo, Y. J.; Sun, J.; Li, G. P. Preparation and Properties of an AP/RDX/SiO_2 Nanocomposite Energetic Material by the Sol-Gel Method. *Propellants, Explos., Pyrotech.* **2012**, *37* (4), 422−426.
(23) Gash, A. E.; Tillotson, T. M.; Satcher, J. H.; Poco, J. F.; Hrubesh, L. W.; Simpson, R. L. Use of Epoxides in the Sol-Gel Synthesis of Porous Iron(Iii) Oxide Monoliths from Fe(Iii) Salts. *Chem. Mater.* **2001**, *13* (3), 999−1007.
(24) Cui, Q. Z.; Jiao, Q. J.; Zhao, W. D. Preparation of Fe_2O_3/CNTs and Its Catalytic Mechanism on Thermal Decomposition of RDX. *Chin. J. Explos. Propellants* **2009**, *32* (4), 68−71.
(25) Peng, D.; Chang, C.; Chiu, M. Thermal Analysis of RDX with Contaminants. *J. Therm. Anal. Calorim.* **2006**, *83* (3), 657−668.
(26) Fathollahi, M.; Mohammadi, B.; Mohammadi, J. Kinetic Investigation on Thermal Decomposition of Hexahydro-1,3,5-Trinitro-1,3,5-Triazine (RDX) Nanoparticles. *Fuel* **2013**, *104*, 95−100.
(27) Gash, A. E.; Satcher, J. H.; Simpson, R. L. Strong Akaganeite Aerogel Monoliths Using Epoxides: Synthesis and Characterization. *Chem. Mater.* **2003**, *15* (17), 3268−3275.